Experiments on Supersonic Turbulent Flow Development in a Square Duct

F. B. Gessner*
University of Washington, Seattle, Washington
S. D. Ferguson†
Boeing Aerospace Company, Seattle, Washington
and
C. H. Lo‡
Spectra Technology Inc., Bellevue, Washington

The nature of supersonic, turbulent, adiabatic-wall flow in a square duct is investigated experimentally over a development length $0 \le x/D \le 20$ for a uniform flow with a Mach 3.9 condition at the duct inlet. The experiments were conducted in a duct that was designed specifically to minimize wave effects and nozzle-induced distortion in the flow. Total pressure contours and local skin friction coefficient distributions show that the flow develops in a manner similar to that observed for the incompressible case. In particular, undulations exist in total pressure contours within the cross plane and in transverse skin friction coefficient distributions, indicating the presence of a well-defined secondary flow superimposed upon the primary flow. The results are analyzed to show that local law-of-the-wall behavior extends well into the corner region, which implies that wall functions conventionally applied in two-equation-type turbulence models, when suitably defined for compressible flow, may also be applied to supersonic streamwise corner flows.

Nomenclature

a = duct half-width, Fig. 8
a' = diagonal half-width, Fig. 8
C = law-of-the-wall constant
C_f = skin friction coefficient, $C_f \equiv 2\tau_w/(\rho_e U_e^2)$
d_o = Preston tube outside diameter
d^+ = dimensionless Preston tube diameter, $d^+ \equiv d_o U_\tau/\nu_w$
D = test section width
L = test section length
m = $[M_e^2(\gamma-1)/2]/[1+M_e^2(\gamma-1)/2]$
M = Mach number
P = pressure
Re' = unit Reynolds number, $Re' \equiv U_e/\nu_e$
U = streamwise velocity
U_τ = friction velocity, $U_\tau \equiv (\tau_w/\rho_w)^{1/2}$
U^* = $(U_e/m^{1/2})\sin^{-1}(m^{1/2}U/U_e)$
x = streamwise coordinate, Fig. 4
y,z = transverse coordinates, Fig. 8
y' = diagonal coordinate, Fig. 8
z_c = centered wall coordinate, Fig. 8
β_k = pressure gradient parameter, $\beta_k \equiv (\delta^*_k/\tau_w)\,\mathrm{d}P/\mathrm{d}x$
δ^*_k = $\int_0^\delta (1-U/U_e)\,\mathrm{d}y$
γ = specific heat ratio
κ = von Karman's constant
μ = absolute viscosity
ν = kinematic viscosity
π = law-of-the-wake coefficient
ρ = density
τ = shear stress

Subscripts

e = boundary-layer edge
cl = centerline value
i = inlet condition
t = total or stagnation condition
w = wall value
2 = pitot probe measured value

Introduction

THIS study was initiated in order to gain a better understanding of the physical nature of developing, supersonic, turbulent flow in a square duct, to compare observed flow behavior with that previously observed in incompressible square duct flows, and to provide data for guiding the development of turbulence models applicable to supersonic corner flows. Previous experimental work related to supersonic turbulent flow in square and rectangular ducts has generally been confined to pressure measurements in the streamwise direction. Richmond and Goldstein,[1] for example, measured streamwise wall static pressure and centerline total pressure distributions in an expanding rectangular duct in order to deduce friction factor and Stanton number behavior for a flow that develops at a nominally constant, core-flow Mach number. In a subsequent study, Merkli[2] examined local pressure recovery behavior in a constant-area, 2:1 aspect ratio rectangular duct by means of wall static pressure and pitot pressure measurements. More recently, Merkli and Abuaf[3] measured streamwise pressure distributions in a supersonic nozzle directly coupled to a constant-area square duct (supersonic diffuser) in order to determine the influence of diffuser length, diaphragm location, and downstream pressure on starting time behavior.

Presented as Paper 86-1038 at the AIAA/ASME Fourth Fluid Mechanics, Plasma Dynamics, and Lasers Conference, Atlanta, GA, May 12–14, 1986; received April 21, 1986; revision received Aug. 22, 1986.

*Professor, Department of Mechanical Engineering. Member AIAA.
†Senior Specialist, Advanced Space Transportation Organization. Member AIAA.
‡Research Scientist, Flow Technology Division.

These studies have provided useful information on the operating characteristics of square and rectangular ducts but have not provided detailed information on local flow behavior in the cross plane, especially in the corner region. In the present paper, data are presented that provide a comprehensive picture of mean flowfield behavior within a constant-area square duct for a supersonic adiabatic-wall flow that develops in the absence of strong internal shock waves from a low-turbulence level, essentially uniform mean flow condition at the duct inlet. The results include total pressure, mean velocity, and Mach number profiles at two streamwise locations, lines of constant total pressure in the cross plane, spanwise wall shear stress distributions, and mean velocity profiles in the near-wall region at different spanwise locations.

Experimental Program

Flow Facility

A continuous-flow, open-circuit wind tunnel was designed and built specifically for the present study. The major components of this facility are shown in Fig. 1. Dry, filtered, high-pressure air (at 276 or 416 kPa, depending on the desired operating Reynolds number) enters the plenum chamber at the ambient total temperature (nominally at 27° C) and then passes through a convergent/divergent nozzle composed of two contoured walls and two parallel side walls. This nozzle accelerates the flow to a Mach 3.9 condition at the start of the test section, which consists of one or more plexiglas square ducts (50.8 × 50.8 mm) connected in a series. The flow exits into a test chamber and expands as a free jet before it enters the intake of a supersonic diffuser. This diffuser is followed by a variable geometry diffuser where a standing normal shock exists downstream of the throat once the tunnel is started. By adjusting the throat of the variable geometry diffuser, it was possible to match the test chamber pressure to the static pressure at the exit plane of the test section before data were taken. The position of the exit plane relative to the test chamber and diffuser intake was fixed, inasmuch as the plenum chamber was mounted on guide rails in order to accommodate ducts of different length. These and other design features of this facility are described in more detail by Ferguson.[4]

Instrumentation

Static pressure data were obtained by means of two sets of wall taps with an orifice size of 0.3 mm located at streamwise intervals $\Delta x/D = 1$ along the test section. On the basis of recent static pressure measurements by Davis[5] in this same facility, it is estimated that the local static pressure was spatially uniform in the cross plane at any streamwise location to within 2% of the wall-measured value. Total pressure distributions were measured at $x/D = 5.37$, 15, and 20 by means of pitot probes constructed from nested stainless steel tubing. One probe with a tip diameter of 0.3 mm was used for measuring total pressure contours in the cross plane (by a searching technique rather than by the interpolation of grid point-measured values). Profile measurements normal to a wall were made with another probe having a flattened tip (0.25 × 0.66 mm outside dimensions). Local wall shear stress (skin friction coefficient) values were determined by means of four different diameter circular pitot tubes (Preston tubes) resting on the wall, with outside diameters ranging from 0.30 to 1.07 mm. For all of these probes, d^+ was always between 30 and 100, which is within acceptable limits on the basis of law-of-the-wall considerations.

The pitot probes were positioned at $x/D = 5.37$ by means of a traversing mechanism used in conjunction with a dial indicator. For measurements with either the $L/D = 15$ or 20 test section in place, the tips of the probes were located approximately 1 mm upstream of the exit plane. These probes were positioned by means of y and z micropositioners located inside the test chamber (Ardel Kinamatic Model T0-100M) which were electrically driven by a remote driver/control unit (Ardel Kinamatic Model C-100-C-2). Pressure measurements were made with a capacitance-type pressure sensor (Barocel Model 570D-1000T) in conjunction with an electronic manometer having a $3\frac{1}{2}$ digit display (Barocel Model 1174). Plenum pressure was measured to within ± 0.1 kPa by means of a well-type mercury manometer (Meriam Model 30 EB25-TM), and plenum stagnation temperature was measured with a mercury-in-glass thermometer to within ± 0.5° C.

Data Reduction Procedures

The local Mach number was calculated from pitot pressure and wall static pressure readings by means of either the isentropic relationship or the Rayleigh-Pitot formula, depending on whether or not P_{t2}/P was greater or less than 1.8929 (M greater or less than unity). The local axial mean velocity was evaluated by employing the quadratic form of the Crocco integral[6] and by assuming that the boundary-layer edge conditions are the same as the conditions on the axial centerline of the duct. This approach was considered acceptable, inasmuch as the value of the pressure gradient parameter for the present study ($\beta_k = 0.1$) is close to that for adiabatic-wall, zero-pressure gradient flow ($\beta_k = 0$). The recovery factor for the mean velocity calculations was specified as 0.89 on the basis of wall temperature measurements by Lo,[7] which also verified the assumption of adiabatic-wall flow. Local skin friction coefficient values were evaluated by means of five different calibration equations that have been proposed for reducing Preston tube data in compressible flow[8-12] as summarized by Lo.[7] Since the calibration equations proposed by Fenter and Stalmach[8] and Bradshaw and Unsworth[10] are implicit in form, a simple bisection-iterative procedure was used to evaluate local skin friction values from these relationships. Additional details of the data reduction procedures and probe configurations are given by Lo.[7]

Preliminary Measurements

Initial data taken with the nozzle directly coupled to the test chamber indicated that the side wall boundary layers were

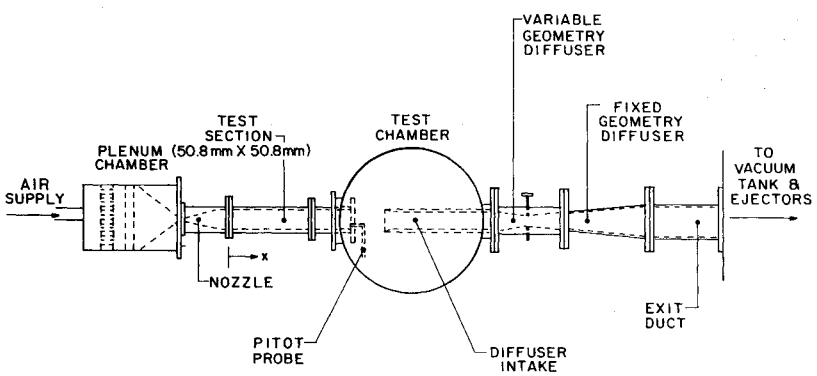

Fig. 1 Schematic diagram of overall flow facility.

distorted at the nozzle exit. This distortion was indicated by an upwelling of lines of constant pitot pressure in the midplane region of each side wall as shown in Fig. 2. With the $L/D = 15$ test section in place, the level of distortion increased downstream of the duct inlet until the pitot pressure contours measured in a quadrant of the flow at the exit plane were distorted as shown in Fig. 3. This behavior was considered unacceptable, inasmuch as pitot pressure contours should be locally symmetric about the corner bisector (CB) of a square duct in a distortion-free flow.

The distortion pattern shown in Fig. 2 is not unique to the present study; it has also been observed in converging rectangular duct flows when the flow is incompressible.[13,14] This distortion arises when transverse pressure gradients in the flow cause a lateral skewing of the flow in the viscous boundary layer relative to that in the inviscid core, with an associated skewing of the vorticity vector that induces axial vorticity in the flow. This explanation is supported by inviscid flow calculations which show that transverse pressure gradients exist downstream of the throat that would tend to promote lateral convergence of the near-wall flow toward the midplane region of each side wall, an effect observed by direct oil flow visualization in the present study.[7] Whether or not this behavior leads to the formation of discrete vortices (secondary flow) superimposed on the primary flow is open to conjecture. It can be said, however, that the distortion evident in Figs. 2 and 3 must have been present to some extent in the studies of Refs. 1–3, all of which utilized a convergent/divergent nozzle composed of two contoured walls and two parallel side walls directly coupled to the duct configuration under investigation.

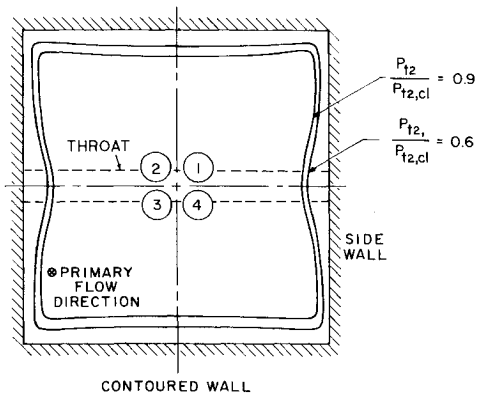

Fig. 2 Pitot pressure contours at nozzle exit, $M = 3.9$, $Re' = 1.2 \times 10^6$/m.

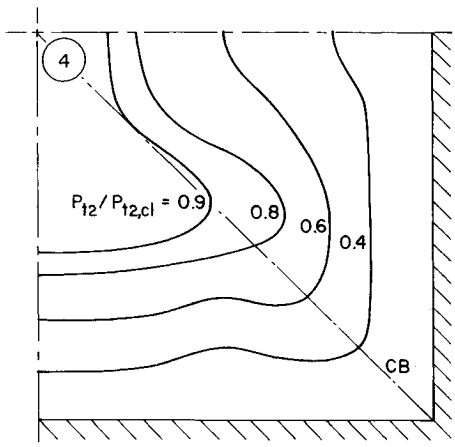

Fig. 3 Pitot pressure contours in a quadrant of the flow at $x/D = 15$, $M_i = 3.9$, $Re_i' = 1.2 \times 10^6$/m.

Test Section Modification

In order to circumvent the distorted flow problem, a smaller, centered square duct made from brass with a 25.4 × 25.4 mm cross section was positioned within a larger plexiglas square duct, as shown in Fig. 4. This configuration enabled the distorted flow at the nozzle exit to be bypassed through the annular space between the inner and outer ducts and new boundary layers to be initiated at the leading edge of each wall of the inner duct, which corresponded to the apex of a 2-deg wedge. The effect of this modification on the local flow symmetry at the exit plane ($x/D = 20$) will be demonstrated. For the moderately high operating unit Reynolds numbers of the present study ($Re_i' = 1.2 \times 10^6$/m and 1.8×10^6/m), turbulent boundary-layer development was initiated at, or very near, the inner duct leading edge, and shock waves induced within the duct were very weak, inasmuch as the inner duct wedge surface immediately downstream of the leading edge was aligned with the primary flow direction (refer to Fig. 4).

Wedge-shaped support plates and variable-length friction plates, acting as spacers between the inner and outer ducts, were positioned as shown in Fig. 4. All wedge-shaped leading and trailing edges were machined to a tip thickness of approximately 0.1 mm and then hand honed to achieve maximum sharpness without "feathering" the edge. Static pressure leads connected to two sets of wall taps along the inner duct were embedded in the duct wall and routed through two of the support plates to the outside. This was done in order not to disturb the flow in the annular space between the inner and outer ducts. The outer duct was also provided with two sets of wall taps along its length. Probe passage through the other two support plates provided access to the inner duct flow at $x/D = 5.37$. By systematically varying the length of the friction plates and the throat width of the variable-geometry diffuser downstream of the diffuser intake (refer to Fig. 1), it was possible to match the inner and outer duct flow static pressures at the exit plane to the test chamber pressure before data were taken. This procedure was followed in order to

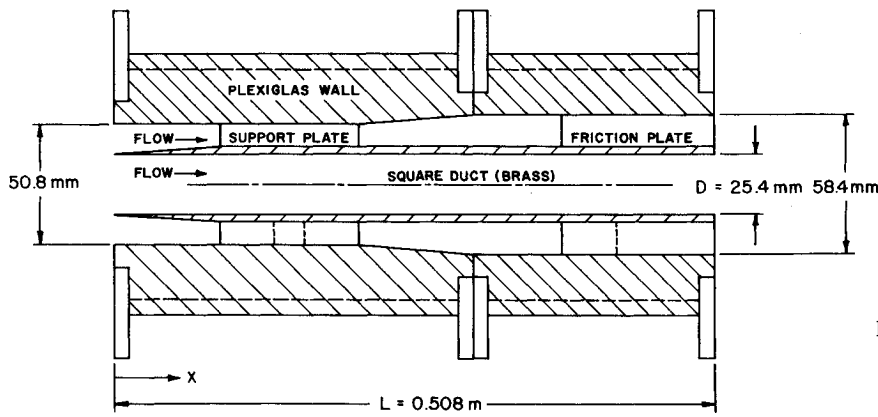

Fig. 4 Schematic diagram of modified test section.

avoid the possible influence of a pressure mismatch on the flow in the subsonic portion of the corner boundary layer immediately upstream of the exit plane.

Results and Discussion

Static Pressure Distributions

Static pressure distributions measured along the inner and outer ducts for matched pressure conditions at the exit plane are shown in Fig. 5. Also shown in this figure are the predicted distributions based on the influence coefficient approach developed by Shapiro[15] and a friction factor that accounts for entry length and oblique shock wave effects.[16] The predicted results show that the slope of the static pressure distribution for the inner duct increases continuously along its length. Although the data appear to follow this trend, close observation of Fig. 5 reveals the presence of slight undulations in the experimental distribution. These undulations are apparently caused by the reflection of weak waves generated at the leading edge of the inner duct and/or by the reflection of waves generated by displacement thickness growth (streamline curvature effects) along the duct. Figure 5 shows that the observed static pressure variation in the annular space between the inner and outer ducts is predicted well by the simple model employed for the calculations. These results also demonstrate the need for an expanding section between the support plates and friction plates in order to obtain matched pressure conditions at the duct exit plane.

Total Pressure Distributions

Total pressure contours measured across the inner duct cross section at $x/D = 20$ for the lower operating Reynolds number are shown in Fig. 6. The results in this figure, when compared to those shown in Fig. 3, indicate that the local flow symmetry was significantly improved when the original test section was replaced by the modified configuration shown in Fig. 4. More specifically, Fig. 6 shows that the flow is now locally symmetric about the corner and wall bisectors of the duct. The undulations appearing in the near-wall contours ($P_t/P_{t,cl} = 0.1$ and 0.2) are similar to those that have been observed in incompressible square duct flow at approximately the same streamwise location.[17,18] These undulations reflect the convecting influence of a secondary flow vortex pair centered about the corner bisector of each quadrant, whose presence was measured in a recent related study.[19] The magnitude and direction of the secondary flow (on the order of 1% of the primary flow) is comparable to that which has been observed in incompressible square duct flow.[20-22]

Although the total pressure contours in Fig. 6 appear to be free of wave reflection effects, these effects are actually present in the flow to some extent. Figure 7 shows the total pressure contours measured in the central region of the duct for the two operating unit Reynolds numbers considered in the present study. At the lower Reynolds number ($Re_i' = 1.2 \times 10^6$/m, Fig. 7a), these contours are relatively undistorted and are similar in appearance to those that have been measured for the incompressible case. At the higher Reynolds number ($Re_i' = 1.8 \times 10^6$/m, Fig. 7b), however, the inner contour ($P_t/P_{t,cl} = 0.95$) has symmetric undulations that are indicative of multiple wave reflections in the duct.

The influence of wave reflections on the flow can be seen more clearly by examining the manner in which total pressure profiles change as the flow develops downstream of the duct leading edge. For this purpose, total pressure profiles measured along the four wall bisector traverses defined in Fig. 8 (y_1 through y_4) will be examined. Profiles measured along these traverses at three streamwise locations for the lower operating Reynolds number are shown in Figs. 9 and 10. In reference to the profiles measured at $x/D = 0$ (refer to Fig. 9), it should be noted that profiles 1 and 3 correspond to profiles measured along traverses normal to the contoured walls of the nozzle, whereas profiles 2 and 4 were measured along traverses normal to the nozzle side walls. This condition accounts, in part, for the profile nonuniformity observed at $x/D = 0$ (nonuniform departures from $P_t/P_{t,cl} = 1$). At $x/D = 5.37$, profiles measured in the inviscid core region reflect the influence of asymmetric compression and expansion waves in the flow. These waves were probably generated at the duct leading edge, where a slightly skewed nozzle exit flow immediately upstream or a slight "cupping" of the very thin, wedge-shaped leading edges would have led to the formation of compression

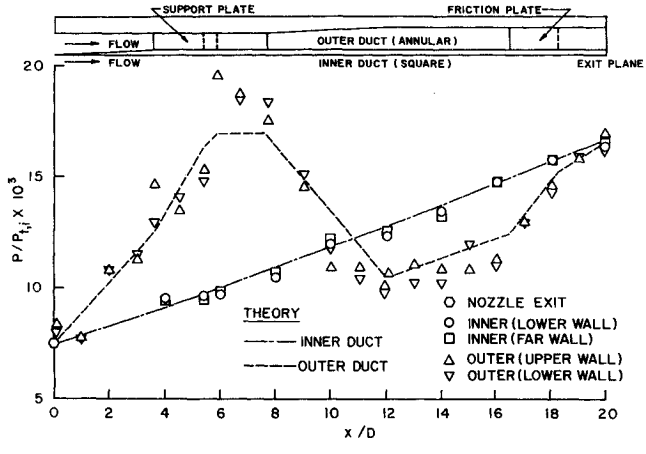

Fig. 5 Axial wall static pressure distributions along the inner and outer ducts, $Re_i' = 1.2 \times 10^6$/m.

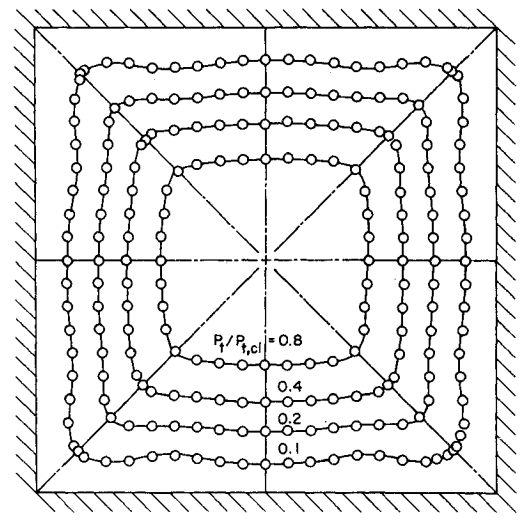

Fig. 6 Total pressure contours across the duct cross section at $x/D = 20$, $Re_i' = 1.2 \times 10^6$/m.

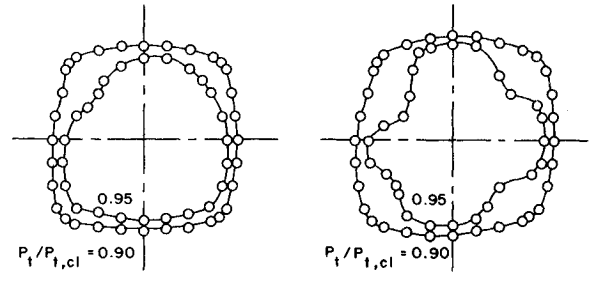

a) $Re_i' = 1.2 \times 10^6$/m. b) $Re_i' = 1.8 \times 10^6$/m.

Fig. 7 Total pressure contours in the central region of the duct cross section at $x/D = 20$.

and expansion waves in the flow. The effect of these waves diminishes in the downstream direction as the boundary layer grows until the total pressure profiles measured at $x/D = 20$ are essentially free of distortion (refer to Fig. 10). These results also show that the duct wall boundary layers have not yet merged at $x/D = 20$ because an inviscid core still exists in the central region of the duct ($P_t/P_{t,cl} \simeq 1$ for $0.7 \leq y_n/a \leq 1.0$). All of these observations also apply for data taken at the higher Reynolds number. For this case, however, profile distortion in the outer region of the flow at $x/D = 5.37$ is more severe than that shown in Fig. 9, but the wall bisector profiles at $x/D = 20$ are similar to those shown in Fig. 10.[7]

Mach Number and Axial Mean Velocity Profiles

Inasmuch as the results shown in Figs. 6, 9, and 10 are indicative of a high degree of local flow symmetry, at least within the viscous layer, the profiles described in this section are all referred to measurements along one wall bisector coordinate and one corner bisector coordinate (y_3 and y', respectively) as defined in Fig. 8. Mach number and axial mean velocity profiles measured along the wall bisector at $x/D = 5.37$ and 20 for the lower Reynolds number case are shown in Fig. 11. The profiles measured at $x/D = 5.37$ (Fig. 11a) are relatively free of distortion in comparison to the total pressure profiles shown in Fig. 9, which implies that multiple wave reflection effects in the duct do not have a significant influence on Mach number and mean velocity profiles in the flow. Profiles measured along the corner bisector at $x/D = 20$ are shown in Fig. 12, where the contour of the dashed-line distribution for the velocity profile in the immediate vicinity of the wall (Fig. 12b) was drawn as shown to satisfy the condition of zero wall shear at the corner. A comparison of the Mach number results in Figs. 11b and 12b shows that the sonic line is close to the bounding wall (below $y/a = 0.01$) in the vicinity of the wall bisector at $x/D = 20$ (Fig. 11b) but is displaced away from the corner on the corner bisector, where subsonic flow exists for $y'/a' < 0.022$ (Fig. 12b). The wall and corner bisector velocity profiles in Figs. 11b and 12a, respectively, indicate that the flow remains wholly attached at $x/D = 20$, even though the flow has developed in the presence of an increasing adverse pressure gradient (refer to Fig. 5). This behavior is different from that for supersonic, laminar, square duct flow, where recent predictions based on the same inlet conditions as those prescribed in the present study have shown that local corner flow separation occurs near $x/D = 17$ and that a partially reversed flow exists along the corner bisector at $x/D = 20$.[23]

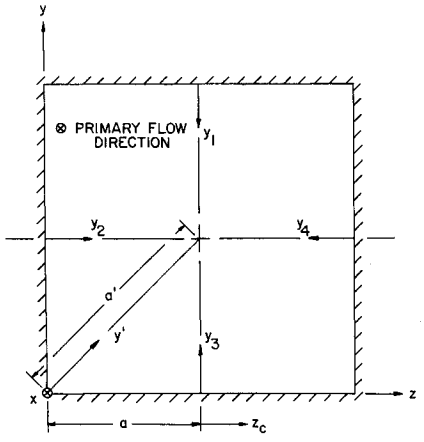

Fig. 8 Reference coordinates.

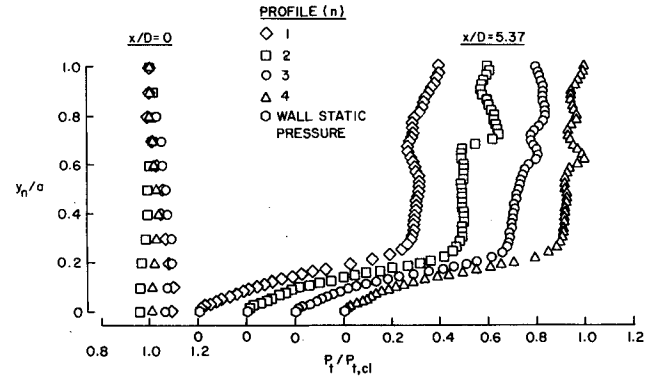

Fig. 9 Total pressure profiles along wall bisectors at $x/D = 0$ and 5.37, $Re_i' = 1.2 \times 10^6$/m.

Local Skin Friction Coefficient Distributions

From a turbulence modelling point of view, the spanwise variation of the local wall shear stress (skin friction coefficient) is of vital interest, inasmuch as this variable appears as a normalizing factor in the wall functions commonly employed in two-equation (e.g., turbulence kinetic energy, dissipation rate) -type turbulence models. Figure 13a shows the spanwise variation of the differential pressure (pitot minus wall static) measured by three different diameter Preston tubes at $x/D = 20$ for the lower operating Reynolds number. These distributions were measured with the probes aligned with the axial flow direction, inasmuch as transverse flow measurements have shown the flow to be locally skewed by less than 4 deg in the near-wall region.[7] The minima and maxima that occur near $z_c/a = 0.5$ and 0.7, respectively, are compatible with the undulations that appear in the total pressure contour shown directly above these distributions. If local law-of-the-wall behavior exists and all three probes were located in the log-law region when data were taken (as will be verified shortly), then the three distributions shown in Fig. 13a should collapse to a common curve when equivalent skin friction coefficient values are calculated via appropriate data reduction formulas (calibration equations).

Figure 13b shows skin friction coefficient distributions corresponding to the data shown in Fig. 13a when the data are reduced by means of five different calibration equations. These equations were developed specifically for reducing Preston tube data in supersonic, adiabatic-wall flows that develop in the presence of mild streamwise pressure gradients. The calibration equations proposed by Sigalla[11] and Hopkins and Keener[12] correspond to the power law forms for the limiting case of incompressible flow, whereas the calibration equations proposed by Fenter and Stalmach,[8] Allen,[9] and Bradshaw and Unsworth[10] are logarithmic in form for this case. In reference to Fig. 13b, it can be seen that the logarithmic-based relationships yield the most consistent results, with Allen's calibration equation providing the least spread in the distributions. On

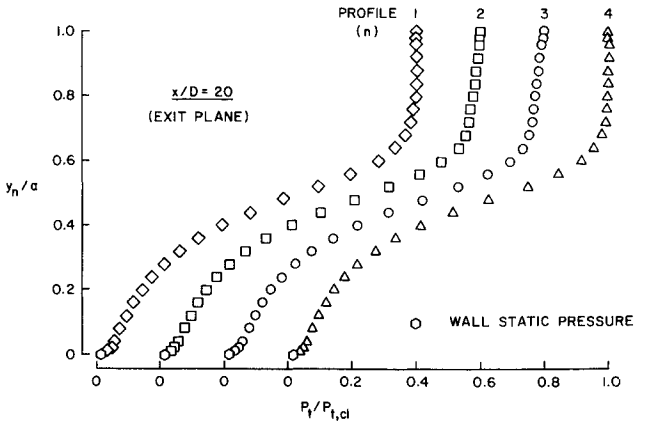

Fig. 10 Total pressure profiles along wall bisectors at $x/D = 20$, $Re_i' = 1.2 \times 10^6$/m.

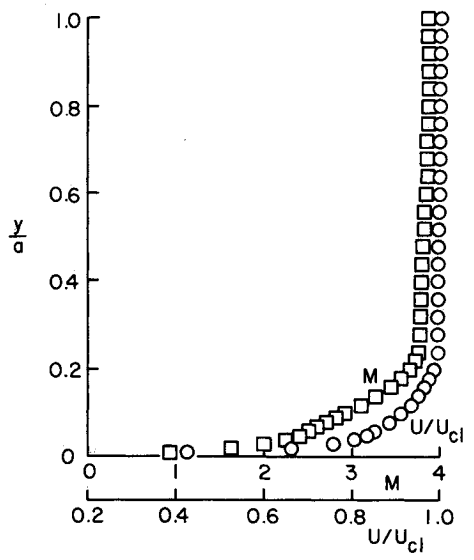

a) $x/D = 5.37$.

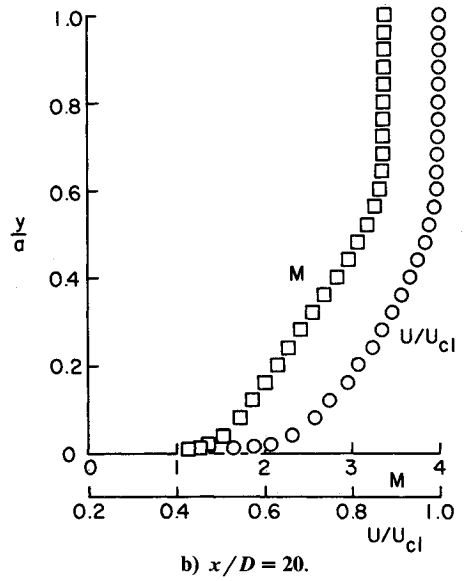

b) $x/D = 20$.

Fig. 11 Mach number and axial mean velocity profiles along a wall bisector, $Re_i' = 1.2 \times 10^6/\text{m}$.

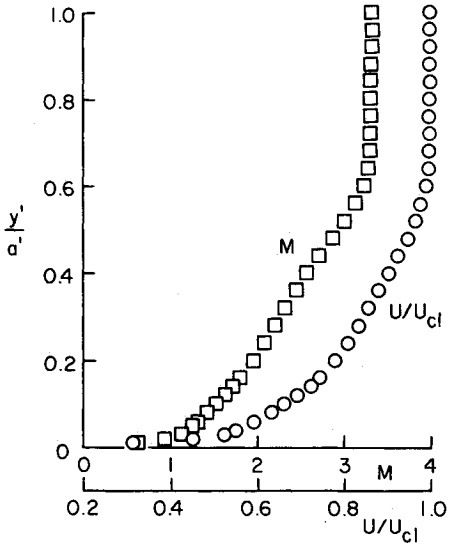

a) Overall profiles.

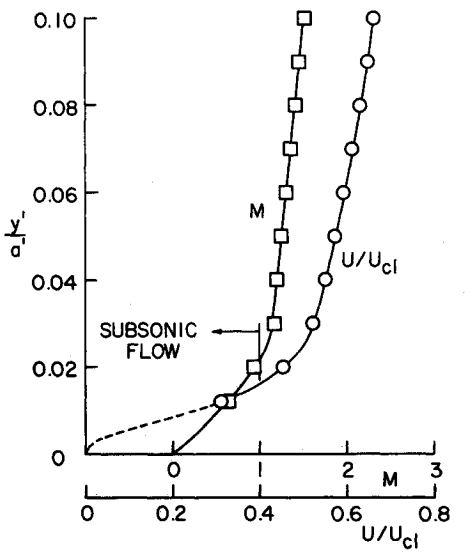

b) Near-wall profiles.

Fig. 12 Mach number and axial mean velocity profiles along a corner bisector at $x/D = 20$, $Re_i' = 1.2 \times 10^6/\text{m}$.

the basis of these results, the three distributions referred to Allen's calibration equation were used to construct the average distribution in Fig. 13b, which also models the average behavior of results referred to Bradshaw and Unsworth's calibration equation quite well.

The undulations that appear in the skin friction coefficient distributions shown in Fig. 13b are similar to those that have been measured in the incompressible square duct flow[17,22] and reflect the convecting influence of the secondary flow. Distributions based on the calibration equations proposed by Sigalla[11] and Hopkins and Keener[12] lie significantly above the average distribution shown in Fig. 13b, especially when based on data taken with the larger diameter Preston tubes (0.635 and 1.067 mm o.d.). This behavior is qualitatively similar to that noted by Collins et al.,[24] who compared skin friction coefficient values based on Preston tube data taken in an adiabatic-wall flow with actual values measured by means of a floating element balance. Their results show that skin friction coefficient values based on the calibration equation proposed by Hopkins and Keener[12] overestimate actual values when $M_e \geq 1$, and that the level of the discrepancy increases as the Mach number increases. On the basis of these observations, Allen's calibration equation was used to calculate local skin friction coefficient values (probe-averaged values) in the present study.

Law-of-the-Wall Velocity Profiles

Velocity profiles measured along a wall bisector at $x/D = 5.37$ and 20 are shown in terms of van Driest-scaled variables for the lower operating Reynolds number in Fig. 14. Also shown in this figure are the d^+ values for the different diameter Preston tubes used to determine the local friction velocity at each location. The line distributions in Fig. 14 represent the law-of-the-wall with κ and C specified as 0.4 and 5.1, respectively. These values were selected because they are representative of typical accepted values and because they provide the best fit of near-wall velocity profile data in incompressible square duct flow.[22] Figure 14 shows that the experimental distributions exhibit log-law behavior at both streamwise locations, with a larger wake component present at $x/D = 20$ by virtue of the stronger adverse pressure gradient at this location (refer to Fig. 5). Similar results were obtained at the higher operating Reynolds number.[7]

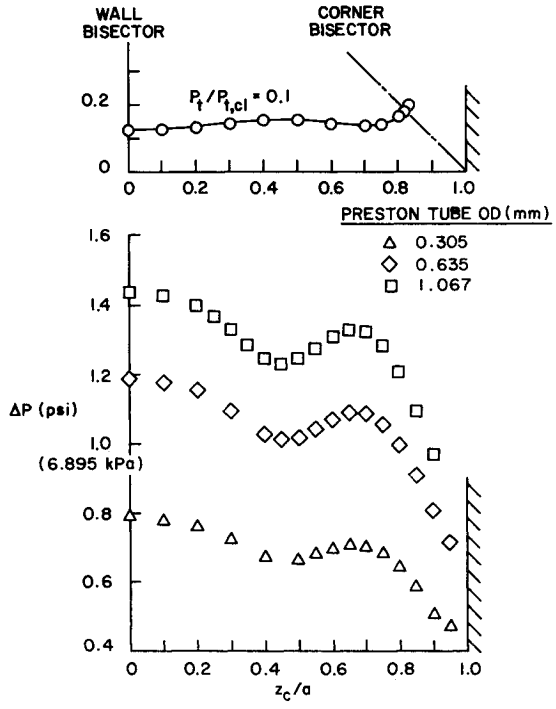

a) Preston tube data.

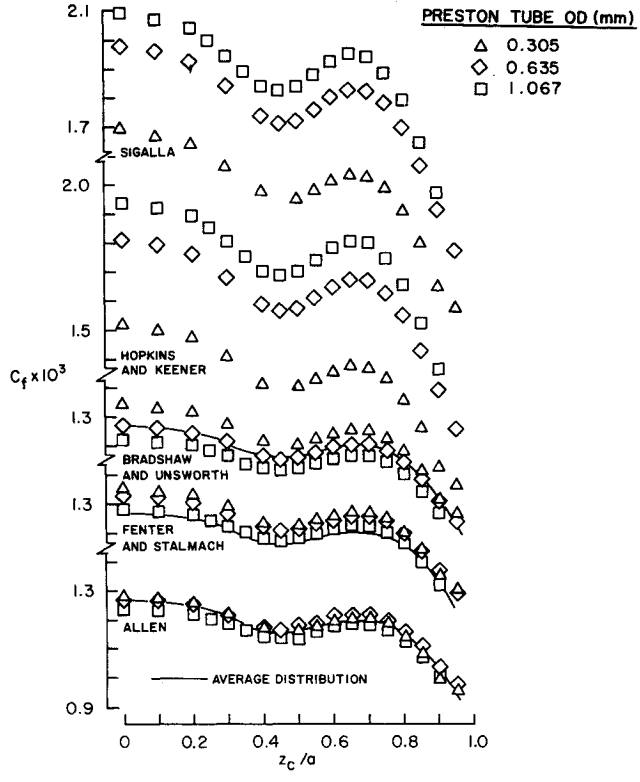

b) Skin friction coefficient distributions.

Fig. 13 Local wall shear stress behavior at $x/D = 20$, $Re_i' = 1.2 \times 10^6$/m.

In order to examine how well local law-of-the-wall behavior extends into the corner region, velocity profiles were measured in the near-wall region ($0 \le y/a \le 0.1$) at different spanwise locations at $x/D = 20$. The results are shown in terms of van Driest-scaled variables for the lower operating Reynolds number in Fig. 15. From the figure it is clear that local law-of-the-wall behavior extends well into the corner region, a result

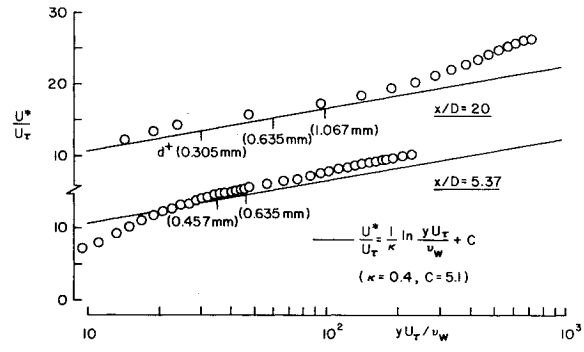

Fig. 14 Velocity profiles along a wall bisector at $x/D = 5.37$ and 20, $Re_i' = 1.2 \times 10^6$/m.

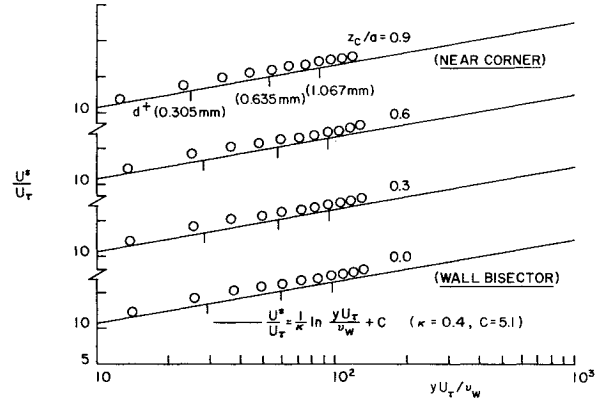

Fig. 15 Velocity profiles in the near-wall region at $x/D = 20$, $Re_i' = 1.2 \times 10^6$/m.

which is compatible with the experimentally observed behavior in incompressible square duct flow.[22] It is also evident, however, that the experimental results in Figs. 14 and 15 lie slightly, but consistently, above the log-law distributions in these figures. In order to investigate possible reasons for this behavior, velocity profiles measured along the wall bisector at $x/D = 20$ for the two operating Reynolds numbers were plotted in defect form as shown in Fig. 16. This figure also includes a line distribution that models experimentally observed behavior in supersonic, adiabatic-wall, flat-plate flow ($\beta_k = 0$)[25] and a line distribution based on a value for the pressure gradient parameter which corresponds to that measured in the present study for the two operating Reynolds numbers ($\beta_k = 0.11$), where the corresponding π values have been taken from Fig. 10 of Ref. 26.

Since the experimental values in Fig. 16 lie consistently above the line distributions, it appears that local friction velocity (U_τ) values may have been underestimated when Allen's calibration equation was used to reduce the Preston tube data. This conjecture is supported by the results of Collins et al.[24] for a Mach 2.2 adiabatic-wall flow, which show that skin friction coefficient values based on Bradshaw and Unsworth's calibration equation (which yields essentially the same results as Allen's calibration equation; refer to Fig. 13b) lie slightly, but consistently, below (by 3 to 5%) the actual values measured with a floating element balance. As further evidence, the skin friction coefficient values based on the calibration equations proposed by Allen[9] and Bradshaw and Unsworth[10] lie consistently below (by approximately 10%) the values calculated from a least-squares-fit of the wall bisector velocity profiles in Fig. 11 to the form of the wall-wake law proposed by Sun and Childs.[27] In this context, it should be noted that if the local skin friction coefficient values specified in the present study are increased by 10%, then the experimental results and line distributions in Figs. 14–16 would agree

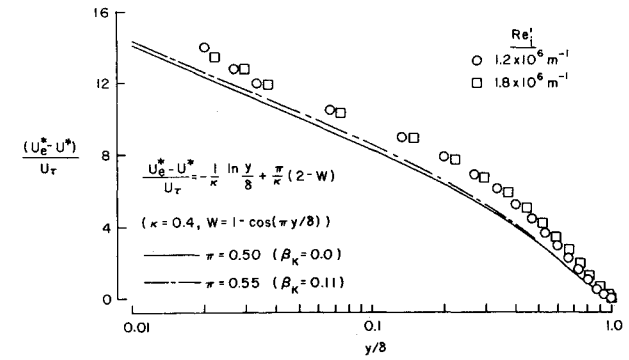

Fig. 16 Velocity defect profiles along a wall bisector at $x/D = 20$.

more closely. On the basis of these observations, it appears that even the most recent calibration equations proposed for reducing Preston tube data in supersonic, adiabatic-wall flows are not entirely adequate, and that further research is necessary in order to develop more accurate data reduction schemes.

Conclusions

The important conclusions that can be drawn from the results of the present study can be summarized as follows:

1) The local mean flowfield associated with developing, supersonic, turbulent, adiabatic-wall flow in a square duct has been investigated experimentally. Data were obtained for a low turbulence level, uniform flow condition at the duct inlet in the absence of compression surface-induced shock waves. Under these operating conditions, the intrinsic effect of the corner dominates the flow, so the data obtained provide a particularly stringent test for corner flow-type turbulence models.

2) Supersonic flow within a square duct develops in a manner similar to that observed for the incompressible case. In particular, undulations exist in total pressure contours within the cross plane and in transverse skin friction coefficient distributions which are indicative of the presence of a well-defined secondary flow superimposed upon the primary flow. Local flow separation was not observed in the near vicinity of the corner, even though the flow develops in the presence of an adverse pressure gradient when the flow is supersonic.

3) Previously proposed, logarithmic-based calibration equations provide an adequate, but not wholly satisfactory, means of reducing Preston tube data taken in supersonic corner flows that develop in the presence of weak secondary flows. Local law-of-the-wall behavior extends well into the corner region, which implies that wall functions conventionally applied to incompressible streamwise corner flows, when suitably defined for compressible flow, may also be applied to supersonic corner flows.

Acknowledgment

This study was sponsored by the Aerodynamics Branch of the NASA Ames Research Center under NASA Grant NGR 48-002-141.

References

[1] Richmond, J.K. and Goldstein, R., "Fully Developed Turbulent Supersonic Flow in a Rectangular Channel," *AIAA Journal*, Vol. 4, Aug. 1966, pp. 1331–1336.

[2] Merkli, P.E., "Pressure Recovery in Rectangular Constant Area Supersonic Diffusers," *AIAA Journal*, Vol. 14, Feb. 1976, pp. 168–172.

[3] Merkli, P.E. and Abuaf, N., "Flow Starting Times in Constant-Area Supersonic Diffusers," *AIAA Journal*, Vol. 15, Dec. 1977, pp. 1718–1722.

[4] Ferguson, S.D., "Design, Fabrication, and Preliminary Measurements in a Supersonic Wind Tunnel for Studying Compressible Turbulent Flow in a Square Duct," MS Thesis, Dept. of Mechanical Engineering, Univ. of Washington, 1979.

[5] Davis, D.O., "Experimental and Numerical Investigation of Steady, Supersonic, Turbulent Flow Through a Square Duct," MS Thesis, Dept. of Mechanical Engineering, Univ. of Washington, 1985.

[6] Cebeci, T. and Smith, A.M.O., *Analysis of Turbulent Boundary Layers*, 1st. Ed., Academic Press, NY, 1974, p. 150.

[7] Lo, C.H., "Mean Flow Measurements in a Square Duct for Supersonic Turbulent Flow Conditions," MS Thesis, Dept. of Mechanical Engineering, Univ. of Washington, 1982.

[8] Fenter, F.W. and Stalmach, C.J. Jr., "The Measurement of Local Turbulent Skin Friction at Supersonic Speeds by Means of Surface Impact Pressure Probes," Rept. CM-878, DRL-392, Univ. of Texas, 1957.

[9] Allen, M.J., "Re-evaluation of Compressible-Flow Preston Tube Calibration Equations in Supersonic Flow," NASA TM X-3488, 1977.

[10] Bradshaw, P. and Unsworth, K., "Comment on 'Evaluation of Compressible-Flow Preston Tube Calibrations'," *AIAA Journal*, Vol. 12, Sept. 1974, pp. 1293–1295.

[11] Sigalla, A., "Calibration of Preston Tubes in Supersonic Flow," *AIAA Journal*, Vol. 3, Aug. 1965, p. 1531.

[12] Hopkins, E.J. and Keener, E.R., "Study of Surface Pitots for Measuring Turbulent Skin Friction at Supersonic Mach Numbers—Adiabatic Wall," NASA TN D-3478, 1966.

[13] Bansod, P. and Bradshaw, P., "The Flow in S-Shaped Ducts," *The Aeronautical Quarterly*, Vol. 23, May 1972, pp. 131–140.

[14] Mokhtari, S. and Bradshaw, P., "Longitudinal Vortices in Wind Tunnel Wall Boundary Layers," *The Aeronautical Journal of the Royal Aeronautical Society*, June/July 1983, pp. 233–236.

[15] Shapiro, A.H., *The Dynamics and Thermodynamics of Compressible Fluid Flow*, 1st Ed., Vol. 1, Ronald Press, NY, 1953, pp. 226–231.

[16] Keenan, J.H. and Neumann, E.P., "Measurements of Friction in a Pipe for Subsonic and Supersonic Flow of Air," *Journal of Applied Mechanics*, Vol. 68, June 1946, pp. A91–A100.

[17] Ahmed, S., "Turbulent Flow in Non-Circular Ducts," Ph.D Thesis, Dept. of Mechanical Engineering, Univ. of Waterloo, Canada, 1971.

[18] Gessner, F.B., Po, J.K., and Emery, A.F., "Measurements of Developing Turbulent Flow in a Square Duct," *Turbulent Shear Flows I*, edited by F. Durst, B.E. Launder, F.W. Schmidt, and J.W. Whitelaw, Springer-Verlag, NY, 1979.

[19] Davis, D.O., Gessner, F.B., and Kerlick, G.D., "Experimental and Numerical Investigation of Supersonic Turbulent Flow Through a Square Duct," *AIAA Journal*, Vol. 24, Sept. 1986, pp. 1508–1515.

[20] Brundrett, E. and Baines, W.D., "The Production and Diffusion of Vorticity in Duct Flow," *Journal of Fluid Mechanics*, Vol. 19, 1964, pp. 375–394.

[21] Melling, A., "Investigation of Flow in Non-Circular Ducts and Other Configurations by Laser Doppler Anemometry," Ph.D Thesis, Univ. of London, 1975; also *Journal of Fluid Mechanics*, Vol. 78, pp. 289–315.

[22] Lund, E.G., "Mean Flow and Turbulence Characteristics in the Near Corner Region of a Square Duct," MS Thesis, Dept. of Mechanical Engineering, Univ. of Washington, 1977.

[23] Davis, D.O., Gessner, F.B., and Kerlick, G.D., "Supersonic Laminar Flow Development in a Square Duct," *AIAA Journal*, to be published.

[24] Collins, D.J., Coles, D.E., and Hicks, J.W., "Measurements in the Turbulent Boundary Layer at Constant Pressure in Subsonic and Supersonic Flow, Part 1. Mean Flow," AEDC-TR-78-21, Jet Propulsion Laboratory, California Institute of Technology, May 1978.

[25] Maise, G. and McDonald, H., "Mixing Length and Kinematic Eddy Viscosity in a Compressible Boundary Layer," *AIAA Journal*, Vol. 6, Jan. 1968, pp. 73–80.

[26] Lewis, J.E., Gran, R.L., and Kubota, T., "An Experiment on the Adiabatic Compressible Turbulent Boundary Layer in Adverse and Favorable Pressure Gradients," *Journal of Fluid Mechanics*, Vol. 51, Pt. 4, 1972, pp. 657–672.

[27] Sun, C.C. and Childs, M.E., "A Modified Wall Wake Velocity Profile for Turbulent Compressible Boundary Layers," *Journal of Aircraft*, Vol. 10, June 1973, pp. 381–382.